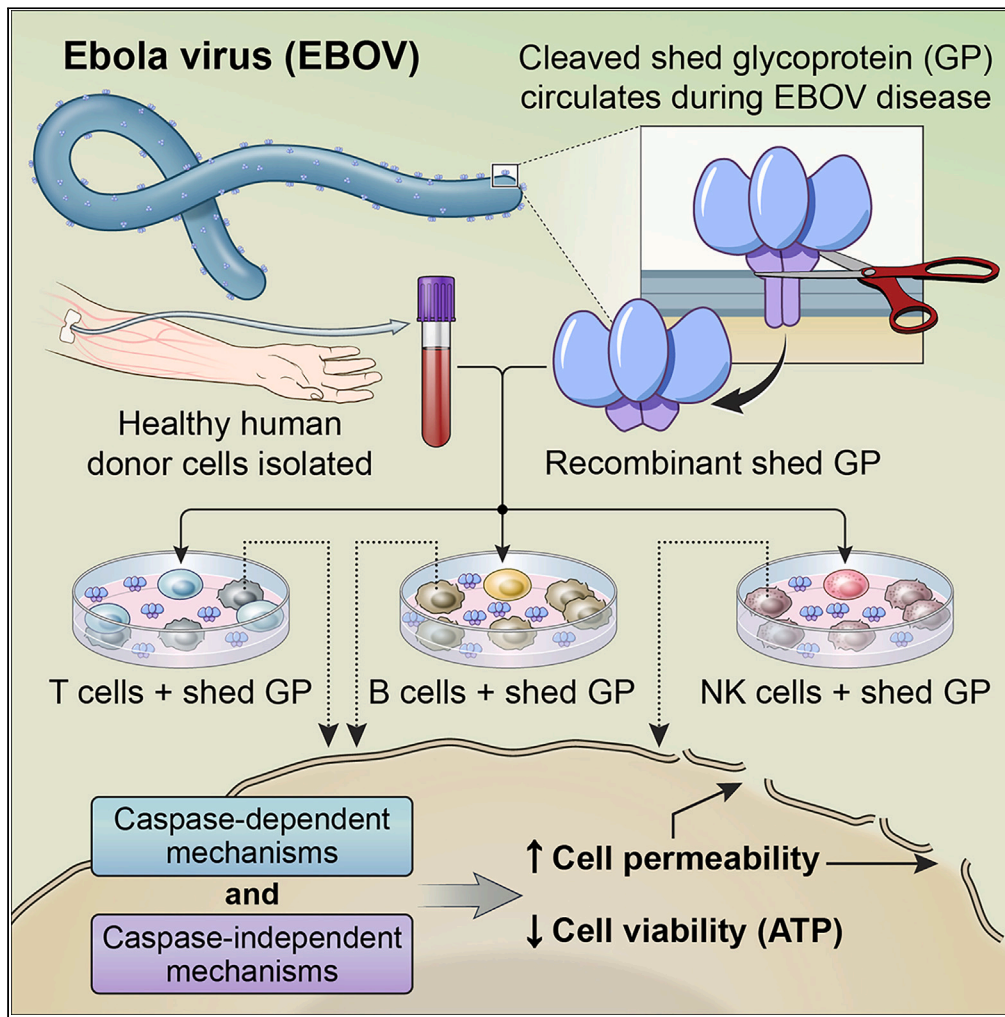


Article

Ebola virus shed glycoprotein is toxic to human T, B, and natural killer lymphocytes



Luis J. Perez-Valencia, Kevin M. Vannella, Marcos J. Ramos-Benitez, ..., Eliana Jacobson, Jason Kindrachuk, Daniel S. Chertow

chertowd@cc.nih.gov

Highlights

EBOV-shed GP consistently decreased viability of human B, NK, and T cells

B and NK cells exhibited higher susceptibility to shed GP than T cells

Continuous kinetics of shed GP-induced cell death differs by cell type

Shed GP-induced cell death is both caspase dependent and caspase independent

Perez-Valencia et al., iScience 26, 107323 August 18, 2023 © 2023 The Author(s). <https://doi.org/10.1016/j.isci.2023.107323>



Article

Ebola virus shed glycoprotein is toxic to human T, B, and natural killer lymphocytes

Luis J. Perez-Valencia,^{1,2,7} Kevin M. Vannella,^{1,2,7} Marcos J. Ramos-Benitez,^{1,2} Junfeng Sun,³ Mones Abu-Asab,⁴ David W. Dorward,⁵ Keytam S. Awad,³ Andrew Platt,^{1,2} Eliana Jacobson,^{1,2} Jason Kindrachuk,⁶ and Daniel S. Chertow^{1,2,8,*}

SUMMARY

Lymphocyte depletion is a distinctive feature of Ebola virus (EBOV) disease. The ectodomain of EBOV glycoprotein (GP) is cleaved off the surface of infected cells into circulation as shed GP. To test the hypothesis that shed GP induces lymphocyte death, we cultured primary human B, NK, or T cells with shed GP *in vitro*. We found that shed GP dependably decreased B, NK, and T cell viability across donors. B and NK cells exhibited higher susceptibility than T cells. Continuous monitoring revealed shed GP began to kill B and NK cells by 4 h and T cells by 5 h. We also demonstrated that shed GP-induced lymphocyte death can be both caspase dependent and caspase independent. Our data are evidence that the cytotoxic effect of shed GP on lymphocytes may contribute to EBOV disease and highlight the need for further research to clarify mechanisms of shed GP-induced death.

INTRODUCTION

Ebola virus (EBOV) is a highly lethal pathogen that causes a critical illness called Ebola virus disease (EVD). Since the discovery of the virus in 1976, there have been sporadic outbreaks with two recent large outbreaks in West Africa (2013–2016) and the Democratic Republic of the Congo (2018–2020).¹ The recurring public health burden of EVD on society emphasizes the importance of further understanding the mechanisms underlying the multifaceted pathogenesis.

EVD pathogenesis includes early immune suppression and inhibition of antiviral responses.² Lymphopenia has been observed in patients with EVD and has been linked to cases of fatal disease, but the mechanisms leading to this depletion remain unclear.^{2–7} Lymphopenia has also been observed in murine and nonhuman primate (NHP) models of EVD.^{8–15} T, B, and natural killer (NK) cells are lymphocytes known to play vital roles in the host response to viruses including EBOV.^{5,8,16–19} Studies reporting lymphocyte counts during EVD in human cases or animal models have consistently reported depletions in T and/or NK cells,^{4–6,8,10,11,14} but to our knowledge B cell counts have only been evaluated in animal models. B cell studies in cynomolgus macaque models of EVD have reported either no depletion¹¹ or slight depletion,¹⁴ and a study in mice reported prominent depletion of B cells.¹⁵

The molecular trigger and underlying mechanisms prompting EBOV-induced lymphopenia remain inconclusive. Infectious EBOV virions have been shown to induce lymphocyte and macrophage death *in vitro*.^{20–22} Apoptosis has consistently been shown to be a means of lymphocyte death in human cases of EVD^{4,5} and in animal models of EBOV infection.^{10,11,20,23,24} As the EBOV glycoprotein (GP) is the only viral protein on the virion surface,²⁵ there have been efforts to describe the role of GP as a critical molecule involved in the immune dysregulation observed in EVD. Other studies suggested that direct GP binding to TLR4 on T cells could contribute to autophagy and abortive infection resulting in T cell depletion.^{22,26} However, both of these reports only considered these phenotypes in T lymphocytes and assessed the role in GP-induced depletion with viral-like particles or infectious virions rather than with purified recombinant protein.

It was shown that the ectodomain of the surface GP can be proteolytically cleaved off infected cells, releasing it into circulation, termed shed GP.²⁷ Shed GP is able to bind to monocytic THP-1 cells facilitating infection and inducing differentiation and death.²⁸ Additionally, shed GP is able to bind neutralizing antibodies suggesting its role as a decoy molecule that interferes with the host humoral response²⁷ and to

¹Emerging Pathogens Section, Critical Care Medicine Department, Clinical Center, National Institutes of Health, Bethesda, MD 20892, USA

²Laboratory of Immunoregulation, National Institute of Allergy and Infectious Diseases, National Institutes of Health, Bethesda, MD 20892, USA

³Critical Care Medicine Department, Clinical Center, National Institutes of Health, Bethesda, MD 20892, USA

⁴Section of Histopathology, National Eye Institute, National Institutes of Health, Bethesda, MD 20892, USA

⁵Microscopy Unit, Research Technology Branch, Rocky Mountain Laboratories, National Institute of Allergy and Infectious Diseases, National Institutes of Health, Hamilton, MT 59840, USA

⁶Laboratory of Emerging Viruses, Department of Medical Microbiology, University of Manitoba, Winnipeg MB R3E 0J9, Canada

⁷These authors contributed equally

⁸Lead contact

*Correspondence:

chertowd@cc.nih.gov

<https://doi.org/10.1016/j.isci.2023.107323>



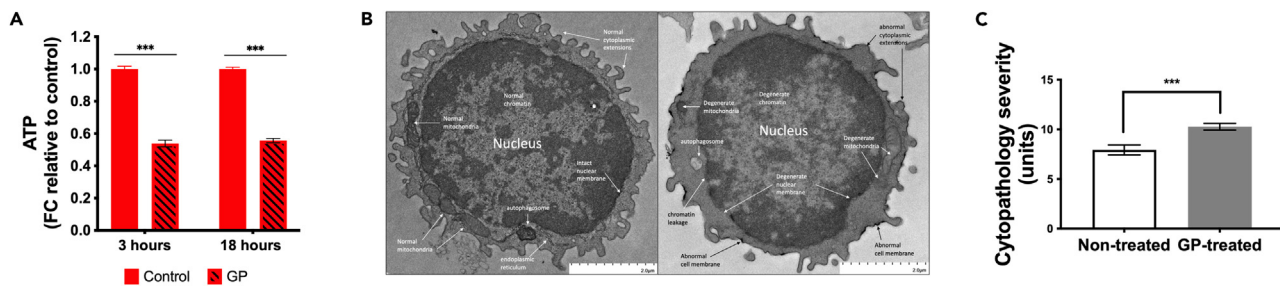


Figure 1. Shed GP reduces T cell viability

(A) Cell viability of primary T cells treated with shed GP (1 μ M) or untreated for 3 h (N = 10 healthy donors) or 18 h (N = 12 healthy donors). Decreased cell viability is represented by lowered ATP levels. SEM bars and T-tests comparing shed GP-treated cells (GP) to untreated cells (control) are shown.

(B) Representative T cell TEM micrographs of non-treated cells (left) showing normal features and shed GP-treated cells (right) showing abnormal features at 6 h post-treatment. Scale bar = 2 μ m.

(C) Blinded scoring of TEM micrographs of non-treated and shed GP-treated T cells at 6 h post-treatment (N = 15 TEM micrographs per condition; 1 healthy donor).

SEM bars are shown. Asterisks reflect T-tests performed to compare between groups. ***p < 0.001.

activate dendritic cells and macrophages through glycosylation-dependent TLR4 signaling.²⁹ It remains unknown if shed GP contributes to the depletion of lymphocytes. Further investigation of a role for shed GP in lymphopenia will yield useful information regarding a critical clinical feature of EVD.

We hypothesized that purified shed GP directly induces lymphocyte death. To test this, we stimulated primary cells with purified recombinant shed GP, assessed the kinetics of cell death, and measured levels of caspase activation. We demonstrated for the first time that shed GP induces T, B, and NK cell death in a time- and dose-dependent fashion. Additionally, we showed that cell death could be partially modulated by inhibiting caspase activation, demonstrating that shed GP induces caspase-dependent and -independent cell death.

RESULTS

Shed GP reduces T cell viability

First, to test the hypothesis that shed GP will reduce T cell viability, we isolated T cells from healthy donor peripheral blood mononuclear cells (PBMCs). We treated T cells with 1 μ M of shed GP and demonstrated that at 3 and 18 h, there was a significant reduction in cell viability caused by shed GP treatment (p < 0.001) (Figure 1A). At 3 h, viability was decreased by 46% and at 18 h by 44% compared to untreated controls. The level of cell viability was similar between 3 and 18 h. This phenotype was consistent across 10 to 12 donors of variable race, sex, and age, suggesting that this is a conserved effect in human T cells. Since the shed GP construct we used contained <1.0 EU per μ g protein of lipopolysaccharide (LPS), we confirmed that up to a 100-fold increase in LPS above 1.0 EU per μ g shed GP did not elicit a similar phenotype induced by shed GP (Figure S1A).

To further understand the effect of shed GP on T cells, we performed transmission electron microscopy (TEM) on untreated T cells and T cells treated with 1 μ M of shed GP for 5 min, 3 h, and 6 h. In comparison to untreated cells, shed GP-treated cells showed more evidence of cell damage and with greater severity at 6 h, as indicated by degeneration in membranes, mitochondria, and chromatin (Figure 1B). We proceeded to quantify the cell damage, utilizing a scoring and point system to characterize the amount of cell damage per cell. Representative images of each condition at each time point were scored after blinding and randomization of the images. We did not observe a significant difference at 5 min or 3 h, but by 6 h of shed GP treatment, we observed a significant difference in the cytopathology scores when compared to untreated cells (Figure 1C).

Shed GP differentially reduces cell viability of B, NK, and T cells

Further expanding on the observation of shed GP-induced reduction of T cell viability, we explored if comparable effects on viability occurred in B cells, NK cells, and total PBMCs which include T cells, B cells, NK cells, monocytes, and dendritic cells. We demonstrated that a 24-h shed GP (1 μ M) treatment resulted in a

significant reduction in B cell, NK cell, and PBMC viability when compared to respective non-treated cells (all cell subsets: $p < 0.001$) (Figure 2A). B cells were the most susceptible to 1 μM concentrations of shed GP (82% decrease in viability) followed by NK cells (67%), PBMCs (53%), and T cells (36%). As a negative control, 24-h treatment with 1 μM soluble (s) GP did not induce death of B cells, NK cells, T cells, or PBMCs (Figure 2B).

To characterize the shed GP dose effect on B cells, NK cells, PBMCs, and T cells, we conducted dose titration experiments using 0.1–2.1 μM shed GP with 3 independent donors (Figure S2). The selected doses showed the dynamic range of the dose effect. Using the data obtained, we estimated the lethal concentration 50 (LC₅₀) by measuring the concentration that resulted in a 50% reduction in cell viability, for each cell subset in each donor. When all donors were combined using a three-parameter log-logistic dose-response model,³⁰ an overall estimated LC₅₀ was calculated for B cells (0.632 μM), NK cells (0.907 μM), PBMCs (1.004 μM), and T cells (1.076 μM) (Figure 2C). The relative consistency among the 3 donors resulted in non-overlapping 95% confidence intervals between the cell subsets.

Shed GP-induced cell death kinetics differ by cell subset

We developed and validated a cell culture system embedded in a microplate reader that facilitated continuous cell culture while simultaneously measuring fluorescence readouts. During assay validation, we used staurosporine as a positive control for T cell death and observed that few untreated cells died during a 24-h period (Figure S3A). This allowed us to expand our analysis beyond endpoint assays and study the kinetics of cell death induced by shed GP. Using our culture system, we cultured B cells, NK cells, PBMCs, and T cells from healthy donors with shed GP (1 μM) and longitudinally measured levels of DNA binding as a correlate of death using a live cell-impermeable fluorescent dye with readouts every 15 min over a 24-h period. Using linear mixed models, we characterized the overall shed GP-induced cell death in the four cell subsets and observed that shed GP-induced cell death progresses differently by cell type (Figures 3A–3D). We determined that the time that cell death reached statistical significance above respective non-treated controls was at 4 h for B cells, NK cells, and PBMCs and 5 h for T cells (Figure 3E). Furthermore, the maximum rate of death for shed GP-treated cell subsets was significantly higher than that of non-treated control cells (all cell subsets: $p < 0.0001$) (Figure S3B). As expected, the cumulative cell death after 24 h showed a significant increase in cell death compared to their corresponding non-treated control. Additionally, we found that the cumulative shed GP-induced cell death effect for PBMCs is significantly smaller than that of B cells ($p = 0.03$), NK cells ($p = 0.002$), and T cells ($p = 0.03$) (Figure 3F). Despite different estimated LC₅₀ values calculated previously, we did not observe significant differences in the cumulative shed GP-induced death effect for B, NK, and T cells over 24 h.

Shed GP increases caspase 3/7 activity in all cell subsets

Previous evidence suggested that caspase activation and apoptosis could be involved in EBOV-induced lymphocyte death.^{4,5,10,11,20–24} Therefore, we explored the role of caspases in shed GP-induced lymphocyte death. We demonstrated that shed GP treatment triggers a significant increase in caspase 3/7 activity in B cells (Fold change (FC): 4.98; $p = 0.009$), NK cells (FC: 6.37; $p < 0.001$), PBMCs (FC: 5.02; $p < 0.001$), and T cells (FC: 3.69; $p < 0.001$) compared to non-treated controls at 3 h (Figure 4). Caspase activity in PBMCs (FC: 1.69; $p < 0.001$) and T cells (FC: 2.94; $p < 0.001$) treated with shed GP remained significantly elevated above non-treated controls when evaluated at 18 h (Figure S4). To rule out LPS-induced caspase 3/7 activation, we demonstrated that up to a 100-fold increase in LPS above 1.0 EU per μg shed GP did not elicit similar activation induced by shed GP (Figure S1B).

Shed GP-induced cell death is caspase dependent and caspase independent

To determine if shed GP-induced cell death was completely mediated by caspase activation, we used a potent pan-caspase inhibitor, Q-VD-Oph (QVD), to determine if we could reverse the shed GP-induced cell death phenotype. We first tested the efficacy of QVD in B cells, NK cells, PBMCs, and T cells. We treated each subset with QVD + GP, and all cell subsets had significantly reduced caspase activation. Caspase activation was reduced to baseline levels similar to controls treated with QVD without GP (Figures S5A–S5D). Q-VE-Oph (QVE), previously validated as a negative control for QVD in Jurkat T leukemia cells,³¹ had a different effect on primary lymphocytes over 24 h. QVE partially reduced caspase activation in B cells, NK cells, T cells, and PBMCs (Figures S5A–S5D). In addition, unlike QVD, QVE was toxic to T cells and NK cells (Figures S6A–S6D).

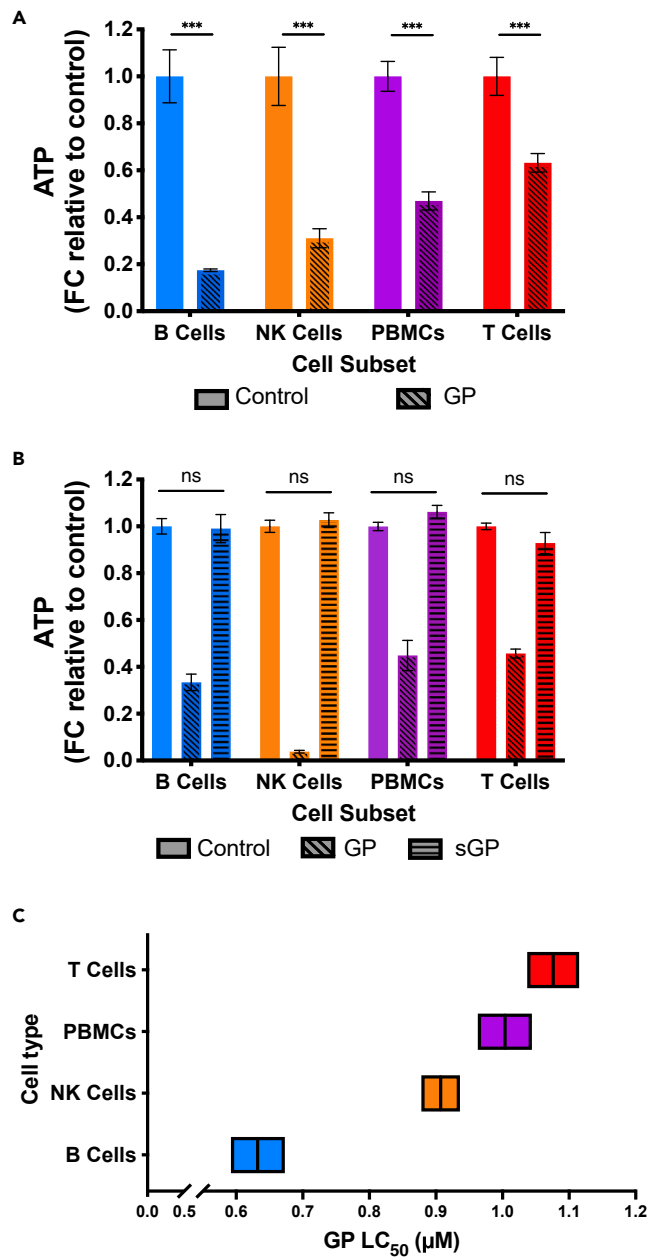


Figure 2. Shed GP reduces viability of B and NK cells more than T cells

(A) Cell viability of primary B cells, NK cells, PBMCs, and T cells treated with shed GP (1 μM) or untreated for 24 h (N = 3 healthy donors). Decreased cell viability is represented by lowered ATP levels. SEM bars are shown. Asterisks reflect T-tests comparing treated cells to untreated control cells. ***p < 0.001.

(B) Cell viability of primary B cells, NK cells, PBMCs, and T cells untreated or treated with shed GP (GP) (1 μM) or soluble (s) GP (1 μM) for 24 h (N = 2 healthy donors). Cell viability represented by ATP levels. T-tests compared ATP produced by untreated cells and sGP-treated cells. ns = not significant.

(C) The concentration of shed GP needed to reduce ATP levels by 50% (LC₅₀). Dose titration experiments with concentrations of shed GP between 0 and 2.1 μM were conducted to determine the LC₅₀ at 24 h in B cells, NK cells, PBMCs, and T cells (N = 3 healthy donors). Overall estimated LC₅₀ represented by a central vertical line with the 95% confidence intervals shown by the width of the box. See Figure S2 for individual titration curves.

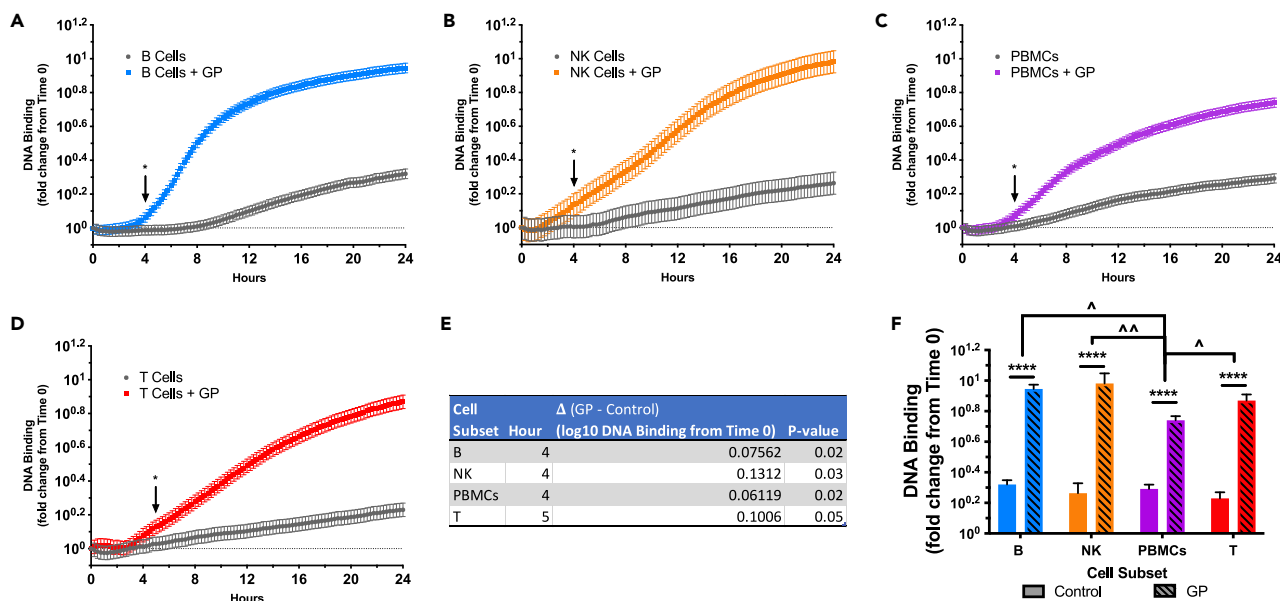


Figure 3. Shed GP-induced cell death progresses differently by cell type

(A–E) Levels of primary cell death are represented by DNA binding of dying cells. Shown are line plots based on estimates from linear mixed models modeling the shed GP-induced lymphocyte death. (A) B cells, (B) NK cells, (C) PBMCs, and (D) T cells were all treated with 1 μ M of shed GP or media for non-treated cells. Fluorescent signals were recorded every 15 min for 24 h. Levels are denoted in fold change units relative to the value measured at zero hours demarcated by the dashed line. The time to onset of death or the earliest time at which shed GP-induced cell death became significantly elevated over controls was determined using linear mixed models and indicated with arrows in (A–D) and in tabular form in (E).

(F) Total cell death after 24 h with shed GP treatment or media. SEM shown with error bars. Two-group comparisons (*) or interaction (^) tests were performed. (N = 3 or 4 healthy donors.) */^: p < 0.05; **/^: p < 0.01; ****: p < 0.0001.

Next, we used our cell culture system to evaluate the cell death kinetics of B cells, NK cells, PBMCs, and T cells treated with either shed GP, shed GP + QVD, QVD alone, or media over a 24-h period. QVD reduced cumulative shed GP-induced death of each cell subset over 24 h (Figure 5A, hashed bars). However, values for shed GP + QVD treatment remained significantly higher when compared to QVD-treated cells (p < 0.0001) indicating that QVD did not fully protect against shed GP-induced death. By comparing QVD-treated and media-treated cells, we also noticed a reduction in baseline death among each cell subset. This reduction was significant in B cells and PBMCs (p < 0.0001), likely associated with prolonged cell culture (Figure 5A, solid bars). However, this was not observed in NK cells or T cells. It is possible that QVD inhibition of baseline cell culture-associated death contributed to the observed protection of shed GP-induced cell death by QVD. Therefore, to account for this, we tested for the possibility of this interaction at each time point (every 15 min) over the 24-h study period.

We identified time points in each cell subset with a significant interaction (p < 0.05), meaning that QVD significantly decreased shed GP-induced cell death beyond the protective effects of QVD on baseline cell death. QVD significantly protected against GP-induced death at all time points between 6.25 and 13.25 h for B cells, 8.25–24 h for NK cells, and 4.75–14.25 h for PBMCs (Figures 5B–5D yellow shading and Excel Table S1). Although we had little evidence of significant interaction in T cells, it is noteworthy that p values remain below 0.10 for the latter 12 h, reaching statistical significance at two time points (15.50 and 16.25 h) suggesting that an interaction effect may have occurred but we did not have enough statistical power to confirm it (Figure 5E yellow shading and Excel Table S1).

Consistent with our initial cumulative death assessment, our analysis of maximum rates of death revealed that QVD significantly reduced the maximum rate of baseline cell death in B cells and PBMCs but not NK cells or T cells (Figure S3C). Rates of death for B cells, NK cells, and PBMCs treated with shed GP + QVD showed a significant reduction when compared to shed GP treatment. However, this was not significant for T cells.

Overall, we observed that inhibiting caspase activation by pre-treating cells with QVD modulates shed GP-induced cell death. Nonetheless, the cell death phenotype was not fully reversed in any cell subset.

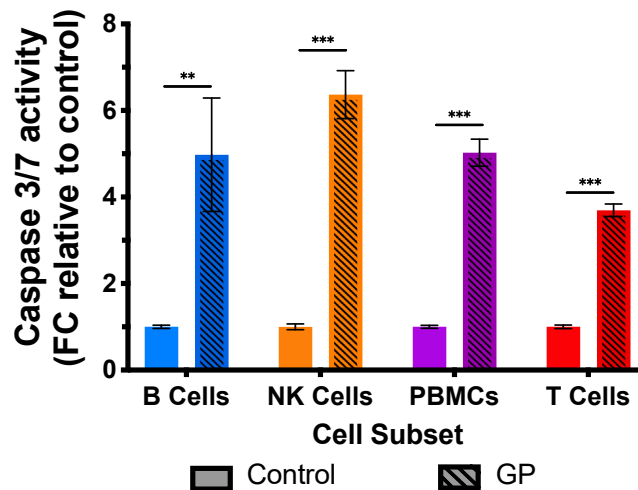


Figure 4. Shed GP induces caspase 3/7 activation

Caspase 3/7 activation from primary B cells, NK cells, PBMCs, and T cells treated with shed GP (1 μ M) or untreated for 3 h. T-tests compared shed GP-treated to non-treated cells. SEM is shown with error bars. B and NK cells (N = 3 healthy donors), PBMCs (N = 6 healthy donors), and T cells (N = 13 healthy donors). **p < 0.01; ***p < 0.001.

DISCUSSION

Previous studies using wild-type virus or pseudotyped viruses bearing the EBOV GP^{21,22} have shown cytotoxic effects on T cells. In this study, we simulated the interaction of circulating shed GP with T cells, B cells, and NK cells by treating primary cells with purified recombinant shed GP. Despite inherent human donor to donor variability, we found that shed GP has a consistent cytotoxic effect on all three cell types. In contrast, sGP did not induce lymphocyte death. sGP is a cleaved precursor to a soluble nonstructural EBOV GP that is secreted in abundance from infected cells and found in serum of infected individuals.^{32,33}

Using the CellTiter-Glo assay (Promega), we measured ATP levels as a surrogate for cell viability. In doing this, we demonstrated that shed GP reduces cell viability of human lymphocytes. The shed GP-dependent reduction in cell viability, or ATP, is in alignment with TEM micrographs of T cells which show degeneration of mitochondria required for aerobic ATP generation. However, the determination of ATP levels could not directly elucidate if and when shed GP induced lymphocyte death. Therefore, we used a separate assay to reinforce our observations.

Using the Victor Nivo (PerkinElmer) we continuously monitored for cell permeability as an indicator of shed GP-induced cell death to fully characterize the death kinetics over 24 h. Our findings showed that given a standard dose of shed GP (1 μ M), shed GP-induced cell death onset did not differ by more than an hour for B cells, NK cells, T cells, and PBMCs. Comparing the overall cell death after a 24-h exposure revealed that the three individual cell subsets were more susceptible to the cytotoxic effect of shed GP than PBMCs. This could be explained by the fact that PBMCs contain monocytes. Monocytes have previously been shown to be activated instead of killed by shed GP.²⁹ The co-culture of the PBMCs together could also be protective against shed GP-induced cell death. Cumulative cell death determinations revealed that there was no statistical difference between the cell death in B cells, NK cells, and T cells. These data may not appear consistent with the cell viability data we obtained from other experiments. There are several possible explanations for this. One is donor-to-donor variability. Another is that the two assays assess different features of cell health. The cell death assay demonstrated that despite similar cumulative cell death among B cells, T cells, and NK cells over 24 h, B cells appear to have a more rapid rate of death earlier than the other cell subsets. This may be reflective of B cells' relatively higher susceptibility to shed GP as determined by the LC₅₀ experiments. There are some limitations to interpreting both assays. The ATP assay reflects a snapshot of the total amount of cytosolic ATP in all cells. While this total ultimately decreases when a cell dies, surviving cells may produce different amounts of ATP which could vary by cell type when they are activated. This is in line with previous literature reporting that remaining lymphocytes are activated during human EVD in the presence of lymphocyte depletion.^{4,18} Different patterns of activated lymphocytes could help

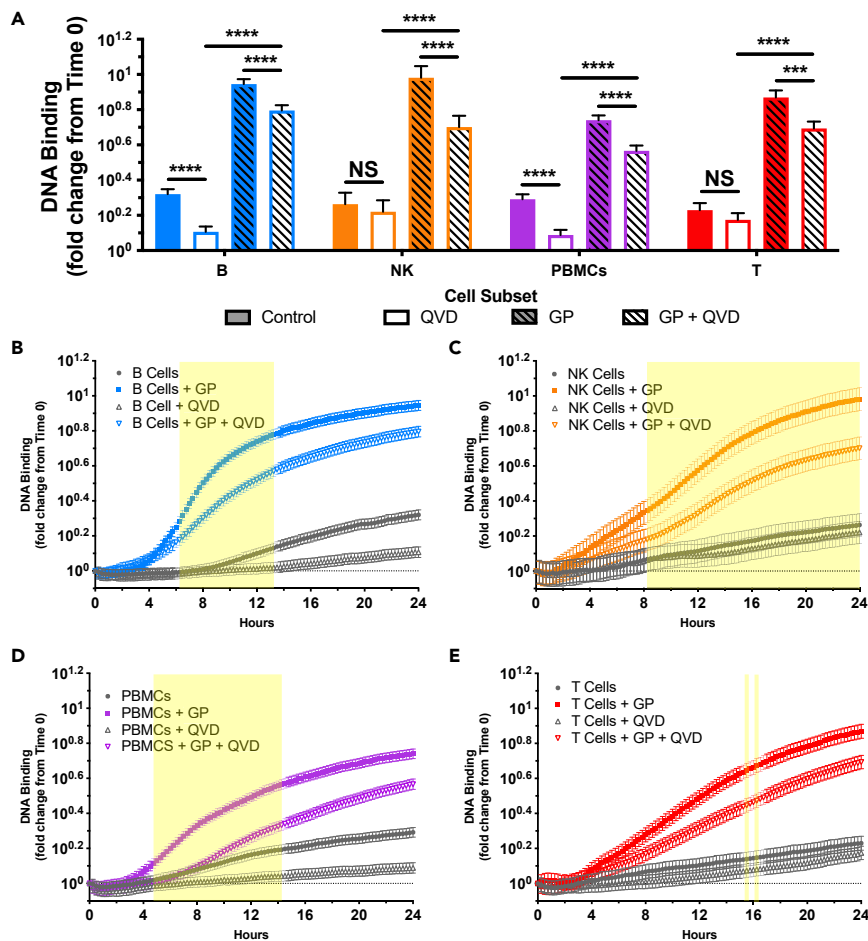


Figure 5. Shed GP-induced cell death is caspase-dependent and -independent

Levels of primary cell death are represented by DNA binding of dying cells. Shown are line plots based on estimates from linear mixed models modeling the shed GP-induced lymphocyte death with or without the pan-caspase inhibitor Q-VD-Oph (10 μ M).

(A) Total cell death after 24 h with or without shed GP treatment and with or without Q-VD-Oph. SEM shown with error bars.

(B–E) B cells, (C) NK cells, (D) PBMCs, and (E) T cells were all treated with 1 μ M of shed GP. Fluorescent signals were recorded every 15 min for 24 h. Levels are denoted in fold change units relative to the reading at time 0 demarcated by the dashed line. Time points that had a significant shed GP and QVD interaction effects were shown on B–E with the yellow background. See Excel Table S1 for interaction effect statistics tables. (N = 3 or 4 healthy donors.) Statistical analysis used linear mixed models. * $p < 0.05$; *** $p < 0.001$; **** $p < 0.0001$.

explain why our results analyzing ATP levels show differences across cell subsets. Additionally, there is a possible limitation in interpretation of the cell death assay. Because we measured cell death over 24 h, it is possible that the DNA-binding reagent is entirely consumed above a certain level of cell death. Collectively, despite these limitations, the two assays demonstrate that shed GP reduces cell viability and causes cell death in human T, B, and NK cells, and we found evidence that B cells and NK cells are more susceptible than T cells.

The underlying mechanisms mediating the kinetics and lethality across the cell subsets remained unclear. Our observation that shed GP-induced lymphocyte death is partially mediated by caspase 3/7 activation is in accordance with past studies showing EBOV-induced lymphocyte death being associated with markers of apoptosis.^{4,5,10,11,20–24} While past literature suggests that this apoptotic phenotype is either mediated through a bystander mechanism triggered by a proinflammatory milieu²⁴ or with direct binding to whole virus,²² our findings suggest that shed GP may also be contributing to caspase activation and apoptosis

of lymphocytes. However, we cannot rule out the possibility that after cells are exposed to shed GP, released cytokines may also have an accessory role in the phenotype we have documented.

Interestingly, using the QVD caspase inhibitor, we showed that shed GP-induced cell death can occur either in a caspase-dependent or caspase-independent manner. The inability to completely revert shed GP-induced cell death with caspase inhibition was not surprising since there is evidence of non-apoptotic mechanisms of cell death including necrosis²² and autophagy²⁶ when cells were exposed to wild-type virus. Also, our finding that the ability to inhibit shed GP-specific caspase-dependent cell death was variable and dependent on cell subset supports the hypothesis that there are cell type-specific mechanisms of death caused by shed GP. After accounting for baseline cell death, the interaction observed in NK cells remained significant until the experiment endpoint suggesting that caspase-driven cell death plays a larger role in shed GP-induced NK cell death than B cell and T cell death at the concentration of shed GP that we used (1 μ M).

A compound called QVE was previously designed to act as a cognate negative control for QVD.³¹ QVE treatment of Jurkat T leukemia cells was reported to be nontoxic and failed to inhibit apoptosis. We were surprised to find that QVE reduced viability of two of the three lymphocyte types that we investigated, and it reduced caspase 3/7 activity by all three lymphocyte types. Consequently, our QVD experiments lacked an appropriate cognate negative control. While this is a limitation in the experimental design, treatment of lymphocytes with QVD demonstrated no adverse effects and consistently reduced caspase 3/7 activation without increasing lymphocyte death.

Shed GP has been found in the blood of EBOV-infected guinea pigs and NHPs.^{27,34} Surprisingly, there have not been previous reports assessing shed GP in the blood or tissues of infected humans. Patients infected with EBOV presumably arrive to Ebola treatment units after they begin to show signs and symptoms. By this time, there has already been considerable viral replication and likely high concentrations of circulating or tissue-localized shed GP that could induce considerable lymphopenia. Our analysis and characterization of shed GP-induced cell death *in vitro* suggests the need for future *in vivo* investigation assessing blood and tissue levels of shed GP in patients with EVD and to determine whether shed GP contributes to lymphopenia in EVD.

Shed GP-induced cell death has further implications on the current knowledge of EVD pathogenesis and suggests that circulating shed GP could impair different levels of the immune response against EBOV. A depletion in T and NK cells, which possess vital roles in immune responses to viruses,³⁵ would compromise the host's ability to mount strong innate and adaptive immunity, allowing the pathogen to replicate in the early stages of infection. Moreover, a depletion in B cells reduces the hosts' ability to mount an effective immune response by impairing antibody production.³⁵ Our findings provide a possible explanation for the NK cell depletion observed in human cases and animal models.^{5,10,11} Although B cell depletion in cases of EVD has only been reported in animal models,^{14,15} we present data that suggest B cells are highly susceptible to shed GP's toxicity and should therefore be analyzed in more depth in future studies.

To further expand our knowledge of shed GP-induced cytotoxicity, important areas of future study could include investigating the role of N-linked and O-linked glycans on the shed GP-induced cell death phenotype. Also, the receptor and signaling used by shed GP to trigger lymphocyte death remains to be addressed. A previous report showed that shed GP does not attach to the surface of T cells.²⁹ Further studies are necessary to understand shed GP structure and how it interacts with lymphocytes to cause death.

In summary, we report that EBOV shed GP is toxic to human T cells, B cells, and NK cells. Additionally, we observed that shed GP-mediated cell death is not limited to a caspase-dependent process. Virus-induced lymphopenia is a profoundly important clinical finding. Lymphopenia is not a phenomenon limited to EVD; it plays an important role in the pathophysiology of viral diseases and merits further research into the mechanisms underlying these cytotoxic effects.

Limitations of the study

As discussed in detail previously, there are limitations to *in vitro* studies designed to model an *in vivo* interaction. While our studies provide the first data about the effects of shed GP on lymphocytes, further

studies are necessary to demonstrate that shed GP-mediated cytotoxicity occurs *in vivo* during EVD. It will be important to document shed GP kinetics in the blood compartment of humans with EVD, and animal models of EVD must be utilized to determine the degree to which shed GP contributes to lymphopenia *in vivo*. More investigations must also be done to define the mechanism by which shed GP interacts with and induces lymphocyte death. Outstanding questions include: does shed GP interact only on the cell surface or is it internalized? What receptor does shed GP interact with? What non-apoptotic type(s) of cell death does shed GP induce? Why do T cells appear to be less sensitive to shed GP than NK cells or B cells? The majority of experiments in this manuscript were conducted with a standard concentration of 1 μM of shed GP. In a small number of experiments, cells treated with higher doses of shed GP produced less ATP and had more caspase activity (Figures S1 and S2). Further experiments will be necessary to understand the impact of varying concentrations of shed GP *in vitro* or *in vivo*. Other limitations to interpretation of the assays and in the experimental designs that we used are also described in detail in the discussion section. We ruled out endotoxin as a cause of lymphocyte death in the shed GP preparation, but we did not test a cell type that was completely protected against shed GP-induced death. A prior study found that shed GP is not cytotoxic to dendritic cells or macrophages, and instead it appears to activate those cell types.²⁹ In the absence of this negative control, it remains a possibility that there is a non-endotoxin component of the recombinant shed GP preparation that has a non-lymphocyte-specific toxic effect.

STAR★METHODS

Detailed methods are provided in the online version of this paper and include the following:

- KEY RESOURCES TABLE
- RESOURCE AVAILABILITY
 - Lead contact
 - Materials availability
 - Data and code availability
- EXPERIMENTAL MODEL AND STUDY PARTICIPANT DETAILS
 - Source and culture of primary human lymphocytes
- METHOD DETAILS
 - Isolation and culture of primary lymphocytes
 - Endpoint analysis of caspase activation and cell viability
 - Estimation of lethal concentration 50 (LC₅₀)
 - Kinetic analysis of cell death
 - Caspase inhibition
 - Transmission electron microscopy (TEM)
- QUANTIFICATION AND STATISTICAL ANALYSIS

SUPPLEMENTAL INFORMATION

Supplemental information can be found online at <https://doi.org/10.1016/j.isci.2023.107323>.

ACKNOWLEDGMENTS

The authors thank S.C. Ramelli for gel electrophoresis materials; S. Alsaaty for help with initial cell purity confirmation; A. Hoofring for assistance with the graphical abstract; and the CCMD members for support, comments, and discussion throughout this project.

This work was supported by the Intramural Research programs of the Clinical Center (NIH) and the National Institute of Allergy and Infectious Diseases (NIH).

The funders had no role in study design, data collection and analysis, decision to publish, or preparation of the manuscript.

The content of this publication does not necessarily reflect the views or policies of the Department of Health and Human Services, nor does mention of trade names, commercial products, or organizations imply endorsement by the U.S. Government.

AUTHOR CONTRIBUTIONS

Conceptualization: L.J.P.-V., M.J.R.-B., E.J., J.K.K., K.M.V., and D.S.C.; Methodology: L.J.P.-V.; Validation: L.J.P.-V., M.J.R.-B., J.S., M.A.-A., K.S.A., A.P., and D.W.D.; Formal Analysis: L.J.P.-V. and J.S.; Investigation: L.J.P.-V., M.J.R.-B., M.A.-A., D.W.D., K.S.A., A.P., and K.M.V.; Resources: J.S., D.W.D., and D.S.C.; Writing-Original Draft: L.J.P.-V., M.J.R.-B., and K.M.V.; Writing- Review & Editing: L.J.P.-V., M.J.R.-B., K.M.V., and D.S.C.; Visualization: L.J.P.-V.; Supervision: J.K.K., K.M.V., and D.S.C.; Funding Acquisition: D.S.C.

DECLARATION OF INTERESTS

The authors declare no competing interests.

INCLUSION AND DIVERSITY

We support inclusive, diverse, and equitable conduct of research.

Received: May 5, 2020

Revised: April 23, 2023

Accepted: July 4, 2023

Published: July 11, 2023

REFERENCES

- Jacob, S.T., Crozier, I., Fischer, W.A., 2nd, Hewlett, A., Kraft, C.S., Vega, M.A.d.L., Soka, M.J., Wahl, V., Griffiths, A., Bollinger, L., and Kuhn, J.H. (2020). Ebola virus disease. *Nat. Rev. Dis. Prim.* 6, 13. <https://doi.org/10.1038/s41572-020-0147-3>.
- Baseler, L., Chertow, D.S., Johnson, K.M., Feldmann, H., and Morens, D.M. (2017). The Pathogenesis of Ebola Virus Disease. *Annu. Rev. Pathol.* 12, 387–418. <https://doi.org/10.1146/annurev-pathol-052016-100506>.
- Younan, P., Iampietro, M., and Bukreyev, A. (2018). Disabling of lymphocyte immune response by Ebola virus. *PLoS Pathog.* 14, e1006932. <https://doi.org/10.1371/journal.ppat.1006932>.
- Agrati, C., Castilletti, C., Casetti, R., Sacchi, A., Falasca, L., Turchi, F., Tumino, N., Bordoni, V., Cimini, E., Viola, D., et al. (2016). Longitudinal characterization of dysfunctional T cell-activation during human acute Ebola infection. *Cell Death Dis.* 7, e2164. <https://doi.org/10.1038/cddis.2016.55>.
- Cimini, E., Viola, D., Cabeza-Cabrerizo, M., Romanelli, A., Tumino, N., Sacchi, A., Bordoni, V., Casetti, R., Turchi, F., Martini, F., et al. (2017). Different features of Vdelta2 T and NK cells in fatal and non-fatal human Ebola infections. *PLoS Neglected Trop. Dis.* 11, e0005645. <https://doi.org/10.1371/journal.pntd.0005645>.
- Wauquier, N., Becquart, P., Padilla, C., Baize, S., and Leroy, E.M. (2010). Human fatal zaire ebola virus infection is associated with an aberrant innate immunity and with massive lymphocyte apoptosis. *PLoS Neglected Trop. Dis.* 4, e837. <https://doi.org/10.1371/journal.pntd.000837>.
- Baize, S., Leroy, E.M., Georges-Courbot, M.C., Capron, M., Lansoud-Soukate, J., Debré, P., Fisher-Hoch, S.P., McCormick, J.B., and Georges, A.J. (1999). Defective humoral responses and extensive intravascular apoptosis are associated with fatal outcome in Ebola virus-infected patients. *Nat. Med.* 5, 423–426. <https://doi.org/10.1038/7422>.
- Bradfute, S.B., Warfield, K.L., and Bavari, S. (2008). Functional CD8+ T cell responses in lethal Ebola virus infection. *J. Immunol.* 180, 4058–4066. <https://doi.org/10.4049/jimmunol.180.6.4058>.
- Ebihara, H., Rockx, B., Marzi, A., Feldmann, F., Haddock, E., Brining, D., LaCasse, R.A., Gardner, D., and Feldmann, H. (2011). Host response dynamics following lethal infection of rhesus macaques with Zaire ebolavirus. *J. Infect. Dis.* 204, S991–S999. <https://doi.org/10.1093/infdis/jir336>.
- Geisbert, T.W., Hensley, L.E., Larsen, T., Young, H.A., Reed, D.S., Geisbert, J.B., Scott, D.P., Kagan, E., Jahrling, P.B., and Davis, K.J. (2003). Pathogenesis of Ebola hemorrhagic fever in cynomolgus macaques: evidence that dendritic cells are early and sustained targets of infection. *Am. J. Pathol.* 163, 2347–2370. [https://doi.org/10.1016/S0002-9440\(10\)63591-2](https://doi.org/10.1016/S0002-9440(10)63591-2).
- Reed, D.S., Hensley, L.E., Geisbert, J.B., Jahrling, P.B., and Geisbert, T.W. (2004). Depletion of peripheral blood T lymphocytes and NK cells during the course of ebola hemorrhagic fever in cynomolgus macaques. *Viral Immunol.* 17, 390–400. <https://doi.org/10.1089/vim.2004.17.390>.
- Fisher-Hoch, S.P., Platt, G.S., Lloyd, G., Simpson, D.I., Neild, G.H., and Barrett, A.J. (1983). Haematological and biochemical monitoring of Ebola infection in rhesus monkeys: implications for patient management. *Lancet* 2, 1055–1058. [https://doi.org/10.1016/s0140-6736\(83\)91041-3](https://doi.org/10.1016/s0140-6736(83)91041-3).
- Reed, D.S., Lackemeyer, M.G., Garza, N.L., Sullivan, L.J., and Nichols, D.K. (2011). Aerosol exposure to Zaire ebolavirus in three nonhuman primate species: differences in disease course and clinical pathology. *Microb. Infect.* 13, 930–936. <https://doi.org/10.1016/j.micinf.2011.05.002>.
- Versteeg, K., Menicucci, A.R., Woolsey, C., Mire, C.E., Geisbert, J.B., Cross, R.W., Agans, K.N., Jeske, D., Messaoudi, I., and Geisbert, T.W. (2017). Infection with the Makona variant results in a delayed and distinct host immune response compared to previous Ebola virus variants. *Sci. Rep.* 7, 9730. <https://doi.org/10.1038/s41598-017-09963-y>.
- Bradfute, S.B., Braun, D.R., Shamblin, J.D., Geisbert, J.B., Paragas, J., Garrison, A., Hensley, L.E., and Geisbert, T.W. (2007). Lymphocyte death in a mouse model of Ebola virus infection. *J. Infect. Dis.* 196, S296–S304. <https://doi.org/10.1086/520602>.
- Dahlke, C., Lunemann, S., Kasonta, R., Kreuels, B., Schmiedel, S., Ly, M.L., Fehling, S.K., Strecker, T., Becker, S., Altfeld, M., et al. (2017). Comprehensive Characterization of Cellular Immune Responses Following Ebola Virus Infection. *J. Infect. Dis.* 215, 287–292. <https://doi.org/10.1093/infdis/jiw508>.
- Ruibal, P., Oestereich, L., Lütke, A., Becker-Ziava, B., Wozniak, D.M., Kerber, R., Korva, M., Cabeza-Cabrerizo, M., Bore, J.A., Koundouno, F.R., et al. (2016). Unique human immune signature of Ebola virus disease in Guinea. *Nature* 533, 100–104. <https://doi.org/10.1038/nature17949>.
- McElroy, A.K., Akondy, R.S., Davis, C.W., Ellebedy, A.H., Mehta, A.K., Kraft, C.S., Lyon, G.M., Ribner, B.S., Varkey, J., Sidney, J., et al. (2015). Human Ebola virus infection results in substantial immune activation. *Proc. Natl. Acad. Sci. USA* 112, 4719–4724. <https://doi.org/10.1073/pnas.1502619112>.
- Warfield, K.L., Perkins, J.G., Swenson, D.L., Deal, E.M., Bosio, C.M., Aman, M.J., Yokoyama, W.M., Young, H.A., and Bavari, S. (2004). Role of natural killer cells in innate protection against lethal ebola virus infection. *J. Exp. Med.* 200, 169–179. <https://doi.org/10.1084/jem.20032141>.

20. Geisbert, T.W., Hensley, L.E., Gibb, T.R., Steele, K.E., Jaax, N.K., and Jahrling, P.B. (2000). Apoptosis induced in vitro and in vivo during infection by Ebola and Marburg viruses. *Lab. Invest.* **80**, 171–186. <https://doi.org/10.1038/labinvest.3780021>.
21. Gupta, M., Spiropoulou, C., and Rollin, P.E. (2007). Ebola virus infection of human PBMCs causes massive death of macrophages, CD4 and CD8 T cell sub-populations in vitro. *Virology* **364**, 45–54. <https://doi.org/10.1016/j.virol.2007.02.017>.
22. Iampietro, M., Younan, P., Nishida, A., Dutta, M., Lubaki, N.M., Santos, R.I., Koup, R.A., Katze, M.G., and Bukreyev, A. (2017). Ebola virus glycoprotein directly triggers T lymphocyte death despite of the lack of infection. *PLoS Pathog.* **13**, e1006397. <https://doi.org/10.1371/journal.ppat.1006397>.
23. Bradfute, S.B., Swanson, P.E., Smith, M.A., Watanabe, E., McDunn, J.E., Hotchkiss, R.S., and Bavari, S. (2010). Mechanisms and consequences of ebolavirus-induced lymphocyte apoptosis. *J. Immunol.* **184**, 327–335. <https://doi.org/10.4049/jimmunol.0901231>.
24. Hensley, L.E., Young, H.A., Jahrling, P.B., and Geisbert, T.W. (2002). Proinflammatory response during Ebola virus infection of primate models: possible involvement of the tumor necrosis factor receptor superfamily. *Immunol. Lett.* **80**, 169–179. [https://doi.org/10.1016/s0165-2478\(01\)00327-3](https://doi.org/10.1016/s0165-2478(01)00327-3).
25. Lee, J.E., and Saphire, E.O. (2009). Ebolavirus glycoprotein structure and mechanism of entry. *Future Virol.* **4**, 621–635. <https://doi.org/10.2217/fvl.09.56>.
26. Younan, P., Santos, R.I., Ramanathan, P., Iampietro, M., Nishida, A., Dutta, M., Ammosova, T., Meyer, M., Katze, M.G., Popov, V.L., et al. (2019). Ebola virus-mediated T-lymphocyte depletion is the result of an abortive infection. *PLoS Pathog.* **15**, e1008068. <https://doi.org/10.1371/journal.ppat.1008068>.
27. Dolnik, O., Volchkova, V., Garten, W., Carbone, C., Becker, S., Kahnt, J., Ströher, U., Klenk, H.D., and Volchkov, V. (2004). Ectodomain shedding of the glycoprotein GP of Ebola virus. *EMBO J.* **23**, 2175–2184. <https://doi.org/10.1038/sj.emboj.7600219>.
28. Iampietro, M., Santos, R.I., Lubaki, N.M., and Bukreyev, A. (2018). Ebola Virus Shed Glycoprotein Triggers Differentiation, Infection, and Death of Monocytes Through Toll-Like Receptor 4 Activation. *J. Infect. Dis.* **218**, S327–S334. <https://doi.org/10.1093/infdis/jiy406>.
29. Escudero-Pérez, B., Volchkova, V.A., Dolnik, O., Lawrence, P., and Volchkov, V.E. (2014). Shed GP of Ebola virus triggers immune activation and increased vascular permeability. *PLoS Pathog.* **10**, e1004509. <https://doi.org/10.1371/journal.ppat.1004509>.
30. Ritz, C., Baty, F., Streibig, J.C., and Gerhard, D. (2015). Dose-Response Analysis Using R. *PLoS One* **10**, e0146021. <https://doi.org/10.1371/journal.pone.0146021>.
31. Southerland, B., Kulkarni-Datar, K., Keoni, C., Bricker, R., Grunwald, W.C., Ketcha, D.M., Hern, E., Cool, D.R., and Brown, T.L. (2010). Q-VE-OPH, a Negative Control for O-Phenoxyl-Conjugated Caspase Inhibitors. *J. Cell Death* **3**, JCD.S4455. <https://doi.org/10.4137/jcd.S4455>.
32. Wolf, K., Beimforde, N., Falzarano, D., Feldmann, H., and Schnittler, H.J. (2011). The Ebola virus soluble glycoprotein (sGP) does not affect lymphocyte apoptosis and adhesion to activated endothelium. *J. Infect. Dis.* **204**, S947–S952. <https://doi.org/10.1093/infdis/jir322>.
33. Furuyama, W., Shifflett, K., Feldmann, H., and Marzi, A. (2021). The Ebola virus soluble glycoprotein contributes to viral pathogenesis by activating the MAP kinase signaling pathway. *PLoS Pathog.* **17**, e1009937. <https://doi.org/10.1371/journal.ppat.1009937>.
34. Rubins, K.H., Hensley, L.E., Wahl-Jensen, V., Daddario DiCaprio, K.M., Young, H.A., Reed, D.S., Jahrling, P.B., Brown, P.O., Relman, D.A., and Geisbert, T.W. (2007). The temporal program of peripheral blood gene expression in the response of nonhuman primates to Ebola hemorrhagic fever. *Genome Biol.* **8**, R174. <https://doi.org/10.1186/gb-2007-8-8-r174>.
35. Flint, S.J., Racaniello, V.R., Rall, G.F., Skalka, A.M., and Enquist, L.W.; American Society for Microbiology (2015). *Principles of Virology*, 4th edition (ASM Press).
36. Offerdahl, D.K., Dorward, D.W., Hansen, B.T., and Bloom, M.E. (2012). A three-dimensional comparison of tick-borne flavivirus infection in mammalian and tick cell lines. *PLoS One* **7**, e47912. <https://doi.org/10.1371/journal.pone.0047912>.

STAR★METHODS

KEY RESOURCES TABLE

REAGENT or RESOURCE	SOURCE	IDENTIFIER
Biological samples		
Primary PBMCs	Healthy human donors	N/A
Chemicals, peptides, and recombinant proteins		
EBOV (subtype Zaire, strain H.sapiens-wt/GIN/2014/Kissidougou-C15) GP	SinoBiological	Cat#40442-V08H2
Recombinant EBOV soluble GP (sGP)	IBT Bioservices	Cat#0565-001
Paraformaldehyde–Glutaraldehyde Solution Karnovsky's Fixative kit	Electron Microscopy Sciences	Cat#15730
LIST HPT LPS from <i>E. coli</i> O113	List Biological Laboratories	Cat#433
Dimethyl sulfoxide	Sigma-Aldrich	Cat#D2650
Staurosporine	Abcam	Cat#ab120056
Q-VD-Oph	Selleckchem	Cat#S7311
Q-VE-Oph	Santa Cruz Biotechnology	Cat#sc-396537
Critical commercial assays		
RealTime-Glo Annexin V Apoptosis and Necrosis Assay	Promega	Cat#JA1011
Caspase-Glo 3/7 Assay Systems	Promega	Cat#G8093
CellTiter-Glo® Luminescent Cell Viability Assay	Promega	Cat#G7571
Software and algorithms		
PRISM	Graphpad Software	Version 7 or 9
R	The R Foundation	Version 3.5.2
Statistical Analysis Software (SAS)	SAS Institute	SAS Institute
Other		
Ficoll-Paque PLUS	GE Healthcare	Cat#17144002
RPMI 1640 Medium	Gibco	Cat#11875-093
HI-FBS	Gibco	Cat#10082-147
Pen-Strep	Gibco	Cat#15140-122
PBS	Gibco	Cat#10010-023
SepMate	StemCell	Cat#85450
EasySep Human T cell Isolation Kit	StemCell	Cat#17951
EasySep Human B Cell Isolation Kit	StemCell	Cat#17954
EasySep Human NK Cell Enrichment Kit	StemCell	Cat#19055
MicroClima Environmental Lid	Labcyte	Cat#LLS-0310-IP
VICTOR Nivo 3S (- dispenser unit/+ gas control unit)	Perkin Elmer	HH35000310
CO2-O2-Controller	Okolab	N/A
1/2 Area ViewPlate-96 well Microplates, PS, TC, White, Sterile	Perkin Elmer	Cat#6005760

RESOURCE AVAILABILITY

Lead contact

Further information and requests for resources and reagents should be directed to and will be fulfilled by the lead contact, Daniel S. Chertow (chertowd@cc.nih.gov).

Materials availability

Materials are available from the [lead contact](#). The study did not generate new unique reagents.

Data and code availability

- All data reported in this paper will be shared by the [lead contact](#) upon request.
- This paper does not report original code.
- Any additional information required to reanalyze the data reported in this paper is available from the [lead contact](#) upon request.

EXPERIMENTAL MODEL AND STUDY PARTICIPANT DETAILS

Source and culture of primary human lymphocytes

Whole blood was obtained from de-identified healthy adult donors according to a clinical protocol approved by the National Institutes of Health Institutional Review Board. Informed consent was obtained from all donors. Donor demographic information for each experiment is found in Excel [Table S2](#). Sample size information is found in Excel [Table S2](#) and the figure legends. All cells were cultured at 37°C and 5% CO₂ in complete media (RPMI 1640 media supplemented with 10% HI-FBS and 1% Pen-Strep (Gibco)).

METHOD DETAILS

Isolation and culture of primary lymphocytes

Peripheral blood mononuclear cells (PBMCs) were isolated using SepMate tubes (StemCell) and Ficoll-Paque PLUS (GE Healthcare) per the manufacturer's recommendations. CD3⁺ T lymphocytes, CD19⁺ B lymphocytes, and CD56⁺ NK lymphocytes were further isolated from PBMCs by negative selection using immunomagnetic bead isolation kits (StemCell). Flow cytometry was used to confirm the purity of isolated cells to be between 94 and 99%. All cells were cultured at 37°C and 5% CO₂ in complete media (RPMI 1640 media supplemented with 10% HI-FBS and 1% Pen-Strep (Gibco)).

Endpoint analysis of caspase activation and cell viability

Caspase activation assay and cell viability assays were performed using the Caspase-Glo 3/7 Assay kit and CellTiter-Glo Luminescent Cell Viability Assay kit, respectively, according to the manufacturer's recommendations (Promega). Complete media, staurosporine (1 μM), Q-VD-Oph (10 μM), Q-VE-Oph (10 μM), sGP (1 μM), and/or shed GP (1 μM) was added to primary cells at the indicated concentrations. Luminescence was measured with a VICTOR Nivo 3S microplate reader (PerkinElmer) at 3, 18, or 24 h.

Estimation of lethal concentration 50 (LC₅₀)

Isolated PBMCs, B cells, NK cells, and T cells were treated with media or escalating doses of GP from 0 μM to 2.1 μM. Cell viability was then determined at 24 h post-treatment with CellTiter-Glo (Promega). To estimate the LC₅₀ for cell death, we used a three-parameter log-logistic dose-response model, which allowed each donor to have a different dose-response curve, but all donors to have the same LC₅₀. The model was fitted using R (The R Foundation, version 3.5.2) package drc (version 3.0–1).³⁰

Kinetic analysis of cell death

Cells were plated into a ½ Area 96 well ViewPlate (PerkinElmer). RealTime-Glo Annexin V Apoptosis and Necrosis Assay (Promega) was prepared at 4x the final concentration and added to cells. Cells with the RealTime-Glo reagent were incubated in a standard laboratory incubator for 2 h per manufacturer's recommendations in order to capture early cell death kinetics. Complete media, staurosporine (1 μM), Q-VD-Oph (10 μM), and/or shed GP (1 μM) was added to primary cells at the indicated concentrations. Fluorescence measurements (indicative of cell membrane permeability and DNA binding) were measured every 15 min using the VICTOR Nivo 3S microplate reader (non-dispenser unit) (PerkinElmer) adapted to a CO₂-O₂-Controller (Okolab). This setup provided us with control over the incubating conditions of 37°C and 5% CO₂. Humidity control was achieved by using the MicroClimate Environmental Lid (Labcyte) per the manufacturer's recommendations to provide a humidity controlled micro-environment within the plate. To further assist with humidity control, surrounding wells and dead space around the wells in use were filled with sterile 1X PBS (Gibco).

The kinetic data were log-transformed and analyzed using linear mixed models to account for repeated measures. The maximum death rates were extracted from loess-smoothed curves of the raw rates using R version 3.5.2. The maximum death rates were then compared using linear mixed models to account for repeated measures. Linear mixed models were fitted using SAS version 9.4 (SAS Institute). Standard residual diagnostics were used to check model assumptions.

Caspase inhibition

The small molecule inhibitor Q-VD-Oph (Selleckchem) and its cognate Q-VE-Oph (Santa Cruz Biotechnology) were reconstituted using DMSO (Sigma-Aldrich) and then diluted in complete media to a final DMSO concentration of $\leq 1\%$.

Transmission electron microscopy (TEM)

T cells were harvested after shed GP or media exposure for 5 min, 3 h, or 6 h. Harvested cells were washed once with PBS. Cells for ultrastructural analysis were re-suspended in a modified Karnovsky's fixative (2% PFA +2.5% glutaraldehyde in 0.1M sodium phosphate 7.2 pH buffer) (Electron Microscopy Sciences). Cells were then placed on ice and sent for further preparation and imaging. Preparation of cells for TEM was performed as described previously³⁶ with the following exceptions. Between each step, cells were centrifuged at $800 \times g$ for 5 min. The cells were embedded in Araldite resin (SPI Supplies) for sectioning at approximately 70 nm. Images were captured at 80 kV on a model H7500 transmission electron microscope (Hitachi High Technologies America), equipped with a model XR100 CCD camera (Advanced Microscopy Techniques). TEM micrographs were taken of 10% of cells that were randomly selected within the viewing area in order to obtain a representative sample of the total population. TEM scoring criteria for ultrastructural analysis and scoring was determined by an electron microscopy expert. TEM micrographs of shed GP- and media-treated T lymphocytes were de-identified and randomized for blinded and unbiased examination ($n = 15$ per condition and time point). The following cellular criteria were scored: 1) cell membrane (present, damaged, absent), 2) cytoplasmic extensions (present, reduced, absent), 3) mitochondrial cristae, (intact, degenerate, absent), 4) endoplasmic reticulum (present, absent), 5) nuclear membrane (intact, damaged, absent), 6) chromatin (pyknotic, normal), 7) chromatin leakage (extranuclear DNA) (present, absent), 8) vesicles (present, absent), 9) autophagosomes (present, absent), 10) protein aggregates (present, absent), 11) glycogen (present, absent), 12) lipid droplets (present, absent), and 13) cell death (present, absent). The scores were statistically analyzed using two-way ANOVAs and standard residual diagnostics were used to check model assumptions with SAS (SAS Institute).

QUANTIFICATION AND STATISTICAL ANALYSIS

All experiments were repeated at least two times. Donor number and biological replicate information can be found for each experiment in the figure legends and Excel [Table S2](#). Graphing and T-test statistical analyses, aside from [Figure S3](#), were performed using PRISM Version 7 or 9 (GraphPad Software). Two-tailed T-test results are specified in the figures and figure legends ($p < 0.05$ was considered significant). Details of other statistical analyses are found in the method details.